

# Magnetic interactions in EuTe epitaxial layers and EuTe/PbTe superlattices

H. Kępa,<sup>1,2,\*</sup> G. Springholz,<sup>3</sup> T. M. Giebultowicz,<sup>2</sup> K. I. Goldman,<sup>2</sup> C. F. Majkrzak,<sup>4</sup> P. Kacman,<sup>5</sup> J. Blinowski,<sup>6,†</sup> S. Holl,<sup>3</sup> H. Krenn,<sup>3,‡</sup> and G. Bauer<sup>3</sup>

<sup>1</sup>*Institute of Experimental Physics, Warsaw University, Hoża 69, 00-681 Warszawa, Poland*

<sup>2</sup>*Physics Department, Oregon State University, Corvallis, OR 97331, USA*

<sup>3</sup>*Institut für Halbleiterphysik, Johannes Kepler University, A-4040 Linz, Austria*

<sup>4</sup>*National Institute of Standards and Technology,*

*Center for Neutron Research, Gaithersburg, MD 20899, USA*

<sup>5</sup>*Institute of Physics, Polish Academy of Sciences, Al. Lotników 32/46, 02-668 Warszawa, Poland*

<sup>6</sup>*Institute of Theoretical Physics, Warsaw University, Hoża 69, 00-681 Warszawa, Poland*

(Dated: November 17, 2018)

The magnetic properties of antiferromagnetic (AFM) EuTe epitaxial layers and short period EuTe/PbTe superlattices (SLs), grown by molecular beam epitaxy on (111) BaF<sub>2</sub> substrates, were studied by magnetization and neutron diffraction measurements. Considerable changes of the Néel temperature as a function of the EuTe layer thickness as well as of the strain state were found. A mean field model, taking into account the variation of the exchange constants with the strain-induced lattice distortions, and the nearest neighbor environment of a Eu atoms, was developed to explain the observed  $T_N$  changes in wide range of samples. Pronounced interlayer magnetic correlations have been revealed by neutron diffraction in EuTe/PbTe SLs with PbTe spacer thickness up to 60 Å. The observed diffraction spectra were analyzed, in a kinematical approximation, assuming partial interlayer correlations characterized by an appropriate correlation parameter. The formation of interlayer correlations between the AFM EuTe layers across the nonmagnetic PbTe spacer was explained within a framework of a tight-binding model. In this model, the interlayer coupling stems from the dependence of the total electronic energy of the EuTe/PbTe SL on the spin configurations in adjacent EuTe layers. The influence of the EuTe and PbTe layer thickness fluctuations, inherent in the epitaxial growth process, on magnetic properties and interlayer coupling is discussed.

PACS numbers: 75.70.Ak, 75.25.+z, 68.65.Cd

## I. INTRODUCTION

In the last decade magnetic multilayer systems and the giant magnetoresistance resulting from interlayer couplings have been receiving considerable interest in both applied and fundamental scientific research. Interlayer exchange couplings in multilayers and superlattices (SLs) have been observed in a large variety of structures composed of metallic ferromagnetic (FM) layers alternating with nonmagnetic metallic<sup>1,2</sup>, as well as nonmetallic<sup>3,4</sup> spacer layers. These observations have stimulated extensive theoretical studies that have resulted in a number of different models for the mechanism of interlayer coupling such as the RKKY model, the free-electron model, and several others. The most complete theory unifying all previous approaches has been devised by Bruno<sup>5</sup>. However, neither interlayer coupling in systems composed of two *nonmetallic* materials, nor mechanisms that might give rise to coupling between *antiferromagnetic* (AFM) layers have been considered in these works.

Yet, neutron diffraction data for three different SL systems composed of AFM and nonmagnetic semiconducting materials, reported in the mid-nineties<sup>6,7,8,9,10</sup>, revealed the existence of pronounced interlayer correlations between the AFM blocks. Also recently, coupling between FM-semiconductor layers has been found in EuS/PbS SLs<sup>11</sup>. In these all-semiconductor systems, the carrier concentration is far too low to support any sig-

nificant RKKY interactions; in addition, the AFM layers do not carry a net magnetic moment. Thus, the two main ingredients which were believed to play a crucial role in interlayer coupling – mobile carriers and layer magnetization – are absent in these cases. These results have clearly demonstrated that the magnetic interlayer coupling is not restricted to structures containing FM metallic components. The proper understanding of correlations between the AFM semiconductor layers may shed new light on the interlayer coupling mechanisms.

In this paper we present our systematic, experimental and theoretical, studies of EuTe epitaxial films and short period [(EuTe)<sub>m</sub>(PbTe)<sub>n</sub>]<sub>N</sub> superlattices. In Section II we describe the basic properties of the constituent materials, sample preparation and the experimental techniques used. The effects of the finite thickness and the strain on magnetic properties of individual layers are treated in Section III. Section IV is devoted to the interlayer coupling determined by neutron diffraction measurements. In its first three subsections, the neutron data for a series of samples studied in zero, intermediate and high magnetic in-plane field, as well as the effect of cooling in external low magnetic field are presented. In the last subsection we discuss the results of a theoretical model for the interlayer coupling in a perfect AFM/nonmagnetic semiconductor SL and we compare the experimental results with the model predictions.

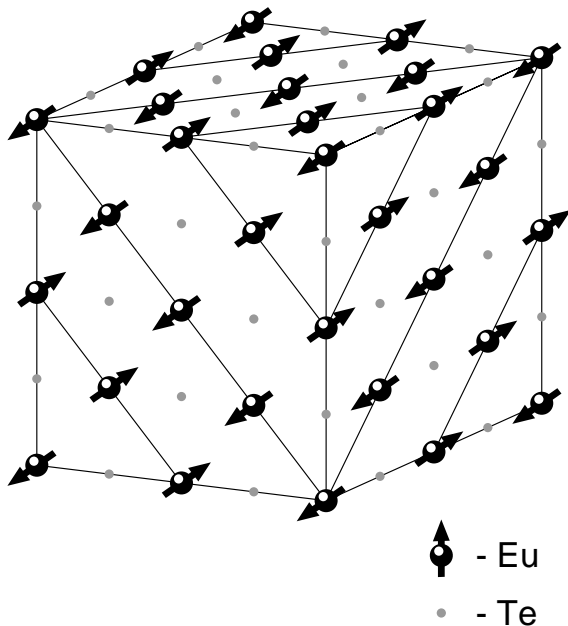


FIG. 1: Chemical and magnetic unit cell of EuTe with its type II AFM structure consisting of ferromagnetically ordered (111) planes and antiferromagnetic spin sequences along the [111] directions.

## II. CONSTITUENT MATERIALS, SAMPLE PREPARATION AND EXPERIMENTAL TECHNIQUES

Bulk EuTe is a classical Heisenberg antiferromagnet with a Néel temperature  $T_N = 9.6$  K<sup>12</sup>. It crystallizes in the NaCl structure with  $a = 6.598$  Å. The  $\text{Eu}^{2+}$  ions with  $S = 7/2$  and  $L = 0$  form an FCC spin lattice with dominant AFM next-nearest neighbor interactions, and weaker FM interaction between the nearest neighbors ( $J_2/k_B = -0.23$  K,  $J_1/k_B = 0.11$  K, respectively<sup>13</sup>). Such a  $J_i$  combination leads to the Type II AFM ordering below  $T_N$ , in which the spins are ferromagnetically ordered in the (111) lattice planes, and the neighboring planes are coupled antiferromagnetically to one another<sup>14</sup> (see Fig. 1). EuTe is a wide gap ( $\sim 2.5$  eV) semiconductor with the  $4f$  levels situated about 2 eV below the conduction band edge<sup>12</sup>. The diamagnetic constituent, PbTe, is a narrow gap ( $\sim 0.19$  eV) semiconductor, which also crystallizes in the NaCl structure and has a bulk lattice constant of 6.462 Å. This yields a close lattice-matching to EuTe, with a mismatch of only 2.1 % in the lattice constants.

The EuTe/PbTe SL samples were grown by molecular beam epitaxy on (111) oriented  $\text{BaF}_2$  substrates as described in detail in Ref. 15. Different  $[(\text{EuTe})_m(\text{PbTe})_n]_N$  SL stacks with  $m$  (varying from 2 to 10) monolayers of EuTe alternating with  $n$  (from 5 to 30) monolayers of PbTe, were deposited on 1 – 3  $\mu\text{m}$  PbTe buffer layers. In the paper the EuTe/PbTe SL with  $m$

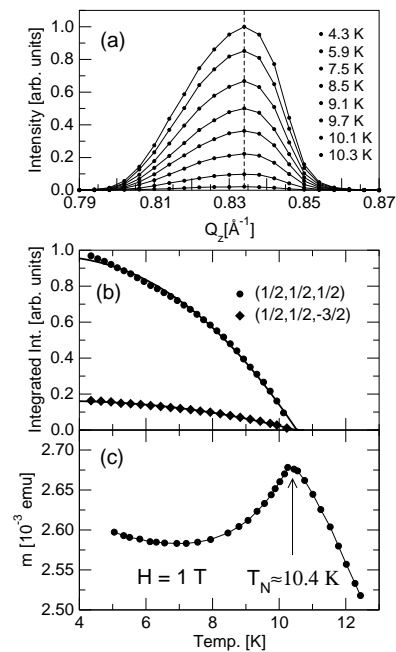


FIG. 2: (a) Evolution of the  $(\frac{1}{2}, \frac{1}{2}, \frac{1}{2})$  magnetic Bragg peak from 3  $\mu\text{m}$  EuTe epilayer with the temperature. The asymmetry of the peak indicates that the relaxation of the strain in the EuTe film is not complete. (b) Integrated intensity of the  $(\frac{1}{2}, \frac{1}{2}, \frac{1}{2})$  and  $(\frac{1}{2}, \frac{1}{2}, \frac{3}{2})$  peaks vs. temperature for the same epilayer. (c) The magnetic moment vs. temperature of 3  $\mu\text{m}$  EuTe epilayer measured by SQUID in applied magnetic field of 1 Tesla.

monolayers of EuTe and  $n$  monolayers of PbTe in the SL period (bilayer) is often denoted by an abbreviated symbol  $(m/n)$ . The thickness of one monolayer is 3.81 Å for EuTe and 3.73 Å for PbTe. To obtain sufficient neutron scattering intensity, the number of periods  $N$  was several hundred in all cases. The layer thicknesses determined by high-resolution x-ray diffraction agreed with the nominal thicknesses within  $\pm 0.5$  monolayer. The electron concentration in the PbTe layers was  $\sim 10^{17} \text{cm}^{-3}$ , i.e., many orders of magnitude lower than in metals, and the EuTe layers were semi-insulating.

The neutron experiments were performed at the NIST Center for Neutron Research. The instruments used were BT-2 and BT-9 triple-axis spectrometers set to elastic diffraction mode, with a pyrolytic graphite (PG) monochromator and analyzer, and a 5 cm PG filter in the incident beam. The wavelength used was  $\lambda = 2.35$  Å and the angular collimation was 40 minutes of arc throughout. Additionally, a number of diffraction experiments were carried out on the NG-1 reflectometer operated at neutron wavelength  $\lambda = 4.75$  Å. The latter instrument yielded a high intensity, high resolution spectra with a negligible instrumental broadening of the SL diffraction lines. All the magnetic diffraction spectra reported here have been measured at 4.3 K.

The dominant feature in diffraction spectra from Type II antiferromagnets is a strong reflection at the  $(\frac{1}{2}, \frac{1}{2}, \frac{1}{2})$

position. Pronounced maxima centered at the  $(\frac{1}{2}\frac{1}{2}\frac{1}{2})$  position were observed in all EuTe and EuTe/PbTe SL samples cooled below the Néel temperature, including those in which the EuTe layer thickness was as small as 2 monolayers. The magnetic origin of the AFM SL peaks was confirmed in several ways. First, the SL reflections also appear at other  $Q$ -space points characteristic for the AFM II structure, their intensities being consistent with the  $\text{Eu}^{2+}$  magnetic formfactor. Secondly, the scattered intensity shows the typical temperature behavior, closely following the squared Brillouin function for a  $S = 7/2$  system below  $T_N$ . Finally, we have performed a number of diffraction measurements in external magnetic fields that convincingly prove the maxima, we have investigated, originate from the ordering of the Eu magnetic moments and not from other effects that may potentially produce peaks at the same reciprocal lattice points (such as, e.g., chemical ordering).

The maxima observed by us show that the Type II AFM ordering was preserved in all EuTe layers and EuTe/PbTe SLs studied. Shown in Fig. 2(a, b) is the temperature dependence of the magnetic peaks intensity for 3  $\mu\text{m}$  EuTe epilayer sample. In Fig. 2(c) the temperature dependence of the magnetic moment of another 3  $\mu\text{m}$  EuTe epilayer measured by a standard SQUID technique is presented<sup>16</sup>. The critical temperatures determined by neutron diffraction and magnetization measurements agree within the experimental errors. The obtained value of  $T_N = 10.4 \pm 0.05$  K is slightly higher than 9.6 K found in bulk EuTe, due to the strain introduced to the epitaxial film by the  $\text{BaF}_2$  substrate and PbTe buffer layer. The distorted, non-gaussian profile of the  $(\frac{1}{2}\frac{1}{2}\frac{1}{2})$  magnetic Bragg peak in Fig. 2a clearly points out to the nonuniform lattice distortions present in the sample, the closer the portions of the EuTe film to the substrate the stronger the deformations of the EuTe lattice. Thus in a sense, the 3  $\mu\text{m}$  layer constitutes only a semi-bulk sample. The influence of strain on magnetic properties of EuTe layers will be discussed in detail in the following section.

### III. STRAIN AND FINITE SIZE EFFECTS

#### A. $T$ -domain structure

In a perfect FCC lattice there are four symmetry-equivalent Type II AFM arrangements in which the FM spin sheets form on the (111),  $(\bar{1}\bar{1}\bar{1})$ ,  $(1\bar{1}\bar{1})$ , or  $(\bar{1}\bar{1}1)$  plane families (see Fig. 3). These four configurations are usually referred to as “ $T$ -domains”. In a macroscopic, strain-free EuTe crystal cooled through the Néel point at  $H_{\text{ext}} = 0$  all four  $T$ -domain states would be populated, giving rise to magnetic peaks at  $(\frac{1}{2}\frac{1}{2}\frac{1}{2})$ ,  $(\frac{\bar{1}}{2}\frac{\bar{1}}{2}\frac{\bar{1}}{2})$ ,  $(\frac{1}{2}\frac{\bar{1}}{2}\frac{\bar{1}}{2})$  and  $(\frac{\bar{1}}{2}\frac{\bar{1}}{2}\frac{1}{2})$  reflection points. However, in the EuTe epilayer and SL samples only the  $(\frac{1}{2}\frac{1}{2}\frac{1}{2})$  maximum is observed in the neutron diffraction spectra; no detectable

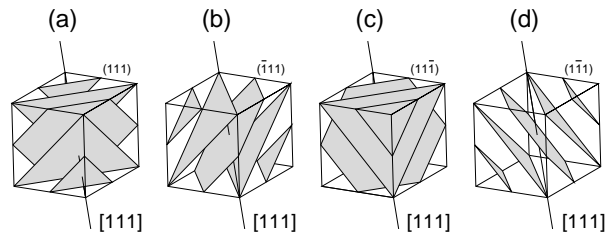


FIG. 3: The four symmetry equivalent Type II AFM arrangements of the  $\{111\}$  ferromagnetic spin sheets in EuTe.

TABLE I: Neighborhood spin configuration in an EuTe layer for different  $T$ -domain types in which the ferromagnetic spin sheets are either parallel (‘in-plane’) or inclined (‘oblique’) to the (111) epitaxial growth plane.

Monolayer number:	Domain type:			
	‘in-plane’		‘oblique’	
	NNs	NNNs	NNs	NNNs
$i - 1$	3(↓)	3(↓)	2(↑)+ 1(↓)	3(↓)
$i$	6(↑)	none	2(↑)+ 4(↓)	none
$i + 1$	3(↓)	3(↓)	2(↑)+ 1(↓)	3(↓)

magnetic scattering was ever found at the other three reflection sites in any of the investigated specimens. This means that in the layer systems only a single  $T$ -domain state forms – the one in which the FM spin sheets are *parallel* to the EuTe layers – whereas the other three ‘oblique’ configurations never occur.

The observed preference in the  $T$ -domain formation can be explained by simple energy arguments. In the Type II AFM structure a spin residing in a given FM sheet has six FM nearest neighbors (NNs) located in the same sheet, and three AFM (‘frustrated’) NNs in each adjacent sheet. The AFM next-nearest neighbors (NNNs) are also located in the adjacent sheets, three in each. Suppose that an (111) EuTe layer consists of  $m$  monolayers. Consider, e.g., an ‘up’ (↑) spin located in the  $i^{\text{th}}$  monolayer. Table I shows its neighbor environment (i.e., how many of its NNs and NNNs with parallel (↑) and antiparallel (↓) spins are located in the  $(i - 1)^{\text{th}}$ ,  $(i)^{\text{th}}$ , and the  $(i + 1)^{\text{th}}$  monolayer) for the ‘in-plane’ and ‘oblique’ domain configurations. Because all NNNs in the Type II AFM structure are antiparallel, the total energy of the NNN interactions is the same in the ‘in-plane’ and the ‘oblique’ domains. The spins residing in monolayers with numbers  $2 \leq i \leq m - 1$  have a full set of six parallel and six antiparallel NNs, so that the total energy of the NN interactions for these spins is zero, regardless of the domain arrangement. However, the spins in the interface monolayers (i.e., those with  $i = 1$  and  $i = m$ ) have only nine magnetic NNs: 6(↑)+3(↓) for the ‘in-plane’ and 4(↑)+5(↓) for the ‘oblique’ domains. Hence, due to the finite thickness of the layer, the exchange energy of the NN spins is not equal to zero any more and different for the

'in-plane' and 'oblique' configurations, with corresponding average magnetic energy per Eu atom of :

$$\epsilon^{\text{in}} = 2C \left[ \frac{-3J_1}{m} + \frac{3(m-1)}{m} J_2 \right] \quad (1)$$

and

$$\epsilon^{\text{obl}} = 2C \left[ \frac{J_1}{m} + \frac{3(m-1)}{m} J_2 \right], \quad (2)$$

where  $C = S(S+1)/3$ . Because  $J_1 > 0$ , the 'in-plane' spin arrangement is the one that minimizes the total magnetic energy.

Another factor that favors the 'in-plane' domain configuration is strain. Since  $a_{\text{PbTe}} < a_{\text{EuTe}}$ , the EuTe lattice is 'compressed' in the layer plane. Therefore the distance  $d_{\text{NN}}^{\parallel}$  between the NN Eu ions located in the same (111) monolayer shortens, while, due to the lattice reaction to the strain the distance  $d_{\text{NN}}^{\text{obl}}$  between the NNs residing in the adjacent (111) monolayers increases. The  $d_{\text{NN}}^{\parallel}$  and  $d_{\text{NN}}^{\text{obl}}$  values may differ from the bulk NN distance  $d_{\text{NN}}^{\text{bulk}}$  by as much as  $\pm 2\%$ . As shown by Goncharenko and Mirabeau<sup>17</sup> from neutron measurements under high hydrostatic pressure, the  $J_1$  exchange constants in Eu chalcogenides generally increases with the decrease of the ion-ion separation. Hence, one can expect the  $J_1^{\parallel}$  for the 'in-plane' NNs to be higher, and the  $J_1^{\perp}$  for the 'out-of-plane' NNs lower than  $J_1^{\text{bulk}}$ . However, for EuTe the rate of  $J_1$  change with  $d_{\text{NN}}$  in the antiferromagnetic state could not be measured in Ref. 17 because the contribution of  $J_1$  to the Néel temperature cancels in the cubic AFM state, i.e.,  $J_1$  is not accessible by experiment under hydrostatic pressure. With respect to the NN exchange,  $J_2$  appears to be only weakly dependent on the ion-ion separation, as shown in Ref. 17.

Taking into account both the finite thickness and strain factors, we obtain the average magnetic energy per Eu spin in EuTe layer consisting of  $m$  monolayers for the two different domain arrangements in the form:

$$\epsilon^{\text{in}} = 2C \left[ -3\Delta J_1 - \frac{3J_1^{\perp}}{m} + \frac{3(m-1)}{m} J_2 \right] \quad (3)$$

and

$$\epsilon^{\text{obl}} = 2C \left[ \Delta J_1 + \frac{J_1^{\perp}}{m} + \frac{3(m-1)}{m} J_2 \right] \quad (4)$$

where  $\Delta J_1 = J_1^{\parallel} - J_1^{\perp}$ .

The first right-side term, which does not depend on the layer thickness, reflects the effect of strain in the observed domain type preference. The second term represents the finite thickness effect as already given in Eq. (1) and (2). In the thick layer limit ( $m \rightarrow \infty$ ) the energy becomes

$$\begin{aligned} \epsilon^{\text{in}} &= 2C[-3\Delta J_1 + 3J_2] \\ \epsilon^{\text{obl}} &= 2C[\Delta J_1 + 3J_2] \end{aligned}$$

which for unstrained samples ( $\Delta J_1 = 0$ ) leads to the bulk value  $\epsilon^{\text{bulk}} = 6CJ_2$  for both arrangements. For small  $m$  values, however, the difference becomes significant (e.g., for  $m = 5$  and  $m = 3$  the energy per spin for the in-plane domain arrangement is lower, respectively, by 8% and 35% than for the oblique ones).

For the in-plane compressed EuTe layers we introduce a parameter which describes the ratio of the elongation of the 'out-of-plane' NNs bonds to the shortening of the distance between the 'in-plane' NNs:  $k = \Delta d_{\text{NN}}^{\text{obl}} / \Delta d_{\text{NN}}^{\parallel}$ . This parameter can be expressed in terms of the in-plane  $e_{\parallel}$  and out-of-plane  $e_{\perp}$  strain, i.e.,

$$k = \frac{1}{e_{\parallel}} \left[ \frac{1}{\sqrt{3}} \sqrt{(1+e_{\parallel})^2 + 2(1+e_{\perp})^2} - 1 \right] \quad (5)$$

For small strain values  $e$ ,  $k$  is essentially constant and directly proportional to the  $e_{\perp}/e_{\parallel}$  ratio. With the value of the Poisson ratio for biaxially strained (111) EuTe layers  $\nu_{111} = 0.301$  and the relation  $e_{\perp}/e_{\parallel} = 2\nu/(\nu-1)$ , we obtain  $k \approx -0.24$  for a compressive in-plane strain values of  $e_{\parallel} \leq 2\%$ .

Using the  $k$  parameter and denoting by  $\xi$  the value of  $(\partial J_1 / \partial d_{\text{NN}})$ , we can rewrite the magnetic energy given by Eq. (3), in the form:

$$\epsilon^{\text{in}} = -6C \left[ \frac{J_1}{m} - \frac{(m-1)}{m} J_2 + \frac{(m(k+1)-1)}{m} \xi d_{\text{NN}} \right] \quad (6)$$

In the EuTe/PbTe structures the compressive strain and finite thickness both appear to favor the 'in-plane' domain arrangement. It is interesting to note, however, that if the spacer material had a larger lattice constant than EuTe and produced a tensile strain in the EuTe layers, the strain would favor the 'oblique' arrangement and the two effects would compete with each other. The domain arrangement in such superlattices could be then tailored by manipulating the EuTe layer thickness.

## B. Changes of the Néel temperature

The effect of the strain and the finite thickness in the EuTe/PbTe system is not only demonstrated by the preferred in-plane spin alignment in the EuTe layers but also substantial shifts in the Néel temperature. This is clearly indicated by the measurements of the intensity of the  $(\frac{1}{2} \frac{1}{2} \frac{1}{2})$  magnetic diffraction signal as a function of temperature as shown in Fig. 4 for several different SL samples with different EuTe layer thicknesses  $m$ . The shapes of these curves were found to be in good agreement with the squared mean-field Brillouin magnetization function for  $S = 7/2$  indicated by the solid lines in Fig. 4. The transition temperature  $T_{\text{N}}$  was determined by fitting the function to the measured data, with  $T_{\text{N}}$  as an adjustable parameter. For most samples the experimental  $T_{\text{N}}$  values differs significantly from the bulk value of  $T_{\text{N}} = 9.6$  K (see Fig. 4).

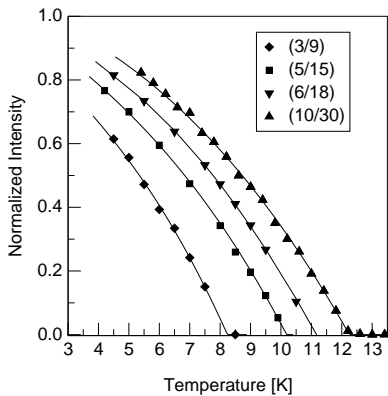


FIG. 4: The intensity of the  $(\frac{1}{2}\frac{1}{2}\frac{1}{2})$  magnetic diffraction peak for different EuTe/PbTe superlattices. The solid lines correspond to the fit with the squared mean field Brillouin magnetization function, with  $T_N$  as an adjustable parameter.

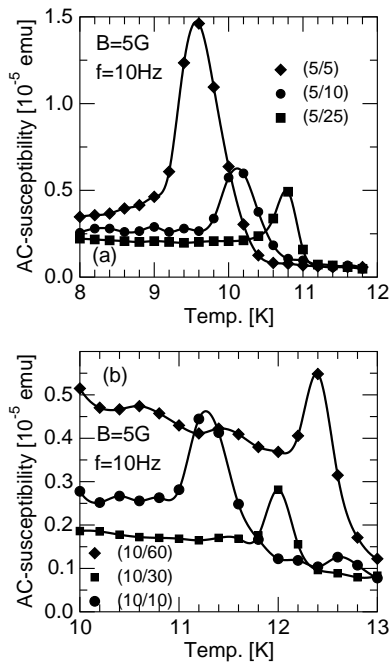


FIG. 5: Magnetic susceptibility of several EuTe/PbTe superlattices measured with 10 Hz AC SQUID magnetometry.

The SL samples were also investigated by magnetometric methods<sup>9</sup>. Examples of the magnetic susceptibility vs. temperature dependence, which was measured using a 10 Hz AC SQUID magnetometer, are shown in Fig. 5 for samples with constant EuTe layer thickness of  $m = 5$  (top panel) and  $m = 10$  (lower panel) but varying PbTe spacer thickness  $n$ . The observed  $\chi(T)$  characteristics for the SL specimens showed distinct maxima indicative for the AFM phase transition. The Néel temperatures obtained by this method were in good agreement (within  $\pm 0.4$  K) with the  $T_N$  values yielded by neutron diffraction experiments.

The analysis of both, the neutron diffraction

and magnetization data for a large number of  $[(\text{EuTe})_m(\text{PbTe})_n]_N$  specimens with different  $m$  and  $n$  values reveals certain distinct trends in the  $T_N$  behavior. The experiments were carried out on series of SL samples for which:

- (i) either the strain in the EuTe layers was approximately constant (by keeping the ratio of  $m$  to  $n$  fixed), see Figs. 4 and 6(a), or
- (ii) the EuTe layer thickness ( $m$ ) was constant, and the PbTe spacer thickness ( $n$ ) varied, see Figs. 5 and 6(b).

In the ‘constant-strain’ samples with very thin EuTe layers ( $m = 2$ ) the  $T_N$  was found to be considerably lower than the bulk value 9.6 K, but it increased with increasing  $m$ . For  $m \approx 5$  it exceeded the  $T_N^{\text{bulk}}$ , showing a tendency to level out at a significantly higher value of 12.6 K (Fig. 6(a)). For the structures with fixed EuTe layer thickness the  $T_N$  showed a clear growing tendency when the PbTe spacer thickness was increased. The larger value of  $n$  for constant  $m$  increases the strain in the magnetic layers. The in-plane strain  $e_{\parallel}$  (or the in-plane lattice constant  $a_{\parallel}$ ) within the EuTe layers was determined by x-ray diffraction. Plotted against  $a_{\parallel}$ , the  $T_N$  data from the sample series with constant  $m$  show approximately linear behavior (Fig. 6(b)).

The trends observed in the  $T_N$  behavior can be explained on the grounds of the same simple model that has been used for explaining the preference in the  $T$ -domain formation. Adopting the mean-field theory approach, one can assume that the phase transition temperature is proportional to the effective field experienced by an ‘average’ spin at  $T = 0$  – in other words, to the average energy per spin  $\epsilon$  in the ground state, given by Eq. (3). Taking into consideration that  $T_N/T_N^{\text{bulk}} = \epsilon/\epsilon^{\text{bulk}}$ , one obtains the expression for the Néel temperature of thick strained layers:

$$T_N = T_N^{\text{bulk}} \left[ 1 + \frac{\Delta J_1}{|J_2|} \right] \quad (7)$$

For small lattice distortions we assume that  $\Delta J_1$  is proportional to the distortion parameter and hence,  $T_N$  should exhibit a linear dependence on the in-plane lattice constant. From the linear fit to the  $m = 10$  data points in Fig. 6(b) we obtain the rate of change of  $T_N$  with  $a_{\parallel}$ :  $\partial T_N/\partial a_{\parallel} = -33.8$  K/ $\text{\AA} \pm 5\%$  and, correspondingly,  $\xi = 0.41$  K/ $(\text{\AA} k_B)$ . For thinner layers, when the  $-6J_1^{\perp}/m$  term may not be neglected, this linear characteristic should shift to the left. This is indeed consistent with the  $T_N$  vs.  $a_{\parallel}$  behavior observed for the  $m = 10$  and  $m = 5$  sample series.

To obtain an expression for  $T_N$  as a function of the distortion parameter  $\Delta d_{NN}^{\parallel}$  and the layer thickness  $m$ , we use as before the  $T_N/T_N^{\text{bulk}} = \epsilon/\epsilon^{\text{bulk}}$  relation with  $\epsilon$  given by Eq. (6):

$$\frac{T_N}{T_N^{\text{bulk}}} = 1 - \frac{1}{m} \left( 1 - \frac{J_1}{|J_2|} \right) + \frac{\xi \Delta d_{NN}^{\parallel} ((k+1)m-1)}{m|J_2|}. \quad (8)$$

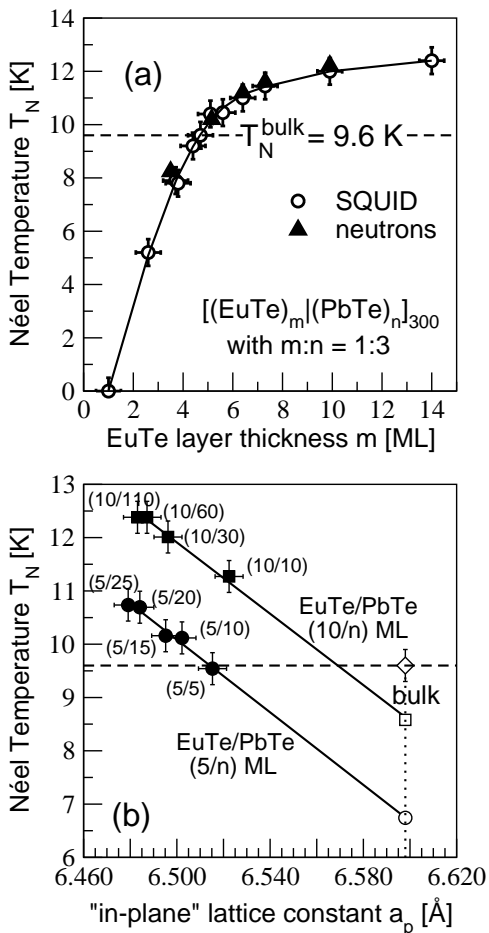


FIG. 6: (a) The Néel temperature for the ‘constant strain’ samples ( $m:n=1:3$ ) vs. EuTe layer thickness. (b) The strain dependence of the Néel temperature for the two families ( $5/n$ ) and ( $10/n$ ) of EuTe/PbTe superlattices. The solid lines are only a guide for the eye.

From Eq. (8) it follows that:

- (i) For samples with the same  $m$ ,  $T_N$  exhibits a linear dependence on  $\Delta d_{NN}^{\parallel}$ .
- (ii) The slope of the  $T_N$  vs.  $\Delta d_{NN}^{\parallel}$  line is equal to  $\xi \Delta d_{NN}^{\parallel} (2m - 1) / m |J_2|$ ; it is weakly dependent on  $m$ , except for very thin layers, where the change in the  $(2m - 1) / m$  factor becomes significant;
- (iii) With decreasing  $m$ ,  $T_N$  shifts to lower values. The ‘zero-strain’  $T_N$  value is given by Eq. (8) by extrapolation to  $\Delta d_{NN}^{\parallel} = 0$ .

The qualitative predictions of the above simple model appear to be consistent with the  $T_N$  vs.  $\Delta d_{NN}^{\parallel}$  measured data for the  $m = 10$  and  $m = 5$  SLs series. The rate of  $J_1$  change yielded by the data appears to be approximately 24% per 1% in the ion-ion distance change. This result supports the conclusions by Goncharenko and Mirabeau<sup>17</sup> concerning the  $J_1$  dependence on distance.

The calculated ‘zero-strain’  $T_N$  for  $m = 10$  and  $m = 5$  is 9.1 K and 8.6 K, respectively, whereas the corresponding values extrapolated from the measured characteristics are 8.5 K and 7.0 K. From Eq. (8) one obtains that the lowest possible Néel temperature is 7.2 K (for unstrained layers with  $m = 2$ ). Actually, experiments on samples with  $m = 2$  yielded  $T_N$  values close to 5 K.

This simple mean-field model correctly explains the qualitative behavior of  $T_N$  in layers with various thicknesses and strain values. However, quantitatively the model appears to be less successful, especially for very thin layers, showing 10% to 20% discrepancy between the model and experimental  $T_N$  values. One possible reason of this discrepancy may be structural imperfections that certainly exist in real superlattices. For instance, as indicated by the results of magnetization studies of EuTe/PbTe(100) SLs<sup>18</sup> and of a similar SL system EuS/PbS<sup>19</sup>, even slight interdiffusion effects in the magnetic/nonmagnetic interface regions may lead to observable decrease of the phase transition temperature due to the reduction of the number of NN and NNN exchange bonds between the Eu spins.

### C. $S$ -domain structure and net magnetic moment

In the model outlined above it was assumed that the Eu spins in each individual EuTe layer form a perfectly homogeneous Type II AFM order. The fact is, however, that in the (111) layer plane there are three  $\langle 11\bar{2} \rangle$  easy axes, 120° apart. This makes possible six microscopically inequivalent domain arrangements (usually referred as the  $S$ -domains<sup>22</sup>). It becomes a natural question whether each individual EuTe layer in the SL structure constitutes a single  $S$ -domain, or does it consist of many smaller ones, in which the spins are oriented along different easy axes. Another important question concerns the magnetic moment of the SL. The layers can be thought of as truly AFM only if  $m$  is an *even* number. For an odd  $m$ , however, the layer as a whole, or the constituent  $S$ -domains should possess an uncompensated moment – in other words, the layers become *ferrimagnetic*. Note, that the opposite spin configurations in successive EuTe layers could also lead to zero net magnetic moment of the entire SL, but this would require strong, perfect interlayer spin correlations.

Information about the  $S$ -domain structure and the net layer moment is important for understanding the inter-layer coupling effects seen in the EuTe/PbTe SLs. There is no direct method of visualizing domains buried in a SL structure or measuring their uncompensated moment. Yet, much insight into both these issues may be obtained from magnetization measurements and from neutron diffraction studies of spin rotation processes in a magnetic field applied parallel to the EuTe layers.

In standard measurements using an unpolarized neutron beam the magnetic diffraction intensity is proportional to  $\cos^2 \alpha$ , where  $\alpha$  is the angle between the spins

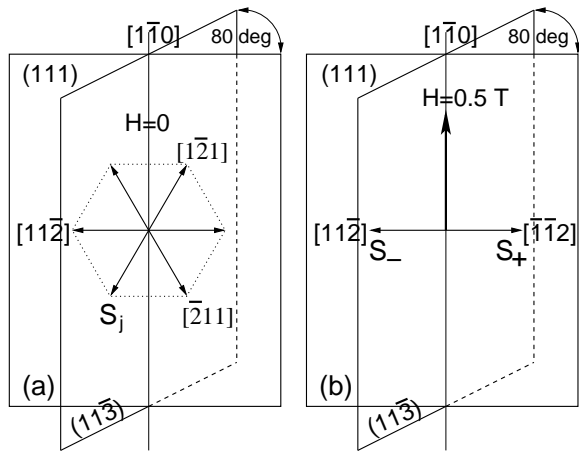


FIG. 7: Directions of Eu spins  $S_j$  in zero external field (a), and in the applied field  $< 1$  T (b).

and the reflecting plane. Since in the EuTe/PbTe systems the spins lie in the (111) plane, for the  $(\frac{1}{2}\frac{1}{2}\frac{1}{2})$  reflection  $\alpha = 0$ . Any spin rotation in the (111) plane does not change this value, and thus the reflection intensity does not change. The information about spin orientation can be obtained from this reflection only by using polarized incident neutrons and polarization analysis of the diffracted beam. However, as the intensity in polarized neutron experiments is typically about an order of magnitude or more lower than in measurements with unpolarized beam, such studies appear to be too time-consuming in the case of the EuTe/PbTe multilayers. Fortunately, the same information can be obtained by studying the  $(\frac{1}{2}\frac{1}{2}\frac{3}{2})$  magnetic reflection, taking advantage of the fact that the reflecting plane associated with it,  $(11\bar{3})$ , is nearly perpendicular to the (111) plane ( $\arccos 1/\sqrt{33} = 80^\circ$ ), see Fig. 7. In such experiments the external field  $\vec{H}_{\text{ext}}$  is applied parallel to the  $[1\bar{1}0]$  axis (i.e., the axis of intersection of the (111) and  $(11\bar{3})$  planes), and the  $(\frac{1}{2}\frac{1}{2}\frac{3}{2})$  reflection intensity is measured vs. the field strength, as shown in Fig. 8.

First, let us discuss the anticipated outcome of such an experiment based on the idealized picture of a EuTe layer. Suppose that all possible  $S$ -domain states are equally populated. Hence, when  $H_{\text{ext}} = 0$ , one-third of all spins are parallel to the  $[11\bar{2}]$  easy axis and make an angle  $\alpha = 80^\circ$  with the  $(11\bar{3})$  plane. Two-third of the spins lie along the  $[\bar{2}11]$  and the  $[1\bar{2}1]$  easy axes (Fig. 7(a)), and for them  $\alpha = 29.5^\circ$ . Thus, the observed reflection intensity is proportional to  $I \propto \frac{1}{3} \cos^2 80^\circ + \frac{2}{3} \cos^2 29.5^\circ = 0.515$ .

When the field is turned on, the system reaction should depend very much on whether the number of spin monolayers is even or odd. Consider first an even  $m$ , so that there is no uncompensated moment. In such a situation, the field tends to turn the spins toward an orientation perpendicular to  $\vec{H}_{\text{ext}}$ . It does not affect the orientation of  $\frac{1}{3}$  of the spins along the  $[11\bar{2}]$  axis which are already perpendicular to  $\vec{H}_{\text{ext}}$ . To turn the remaining  $\frac{2}{3}$  of the

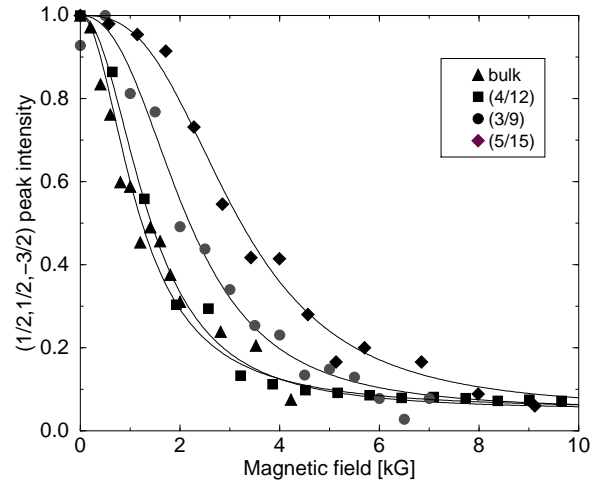


FIG. 8: Intensity of the  $(\frac{1}{2}\frac{1}{2}\frac{3}{2})$  reflection vs. applied magnetic field for a bulk EuTe specimen and several EuTe/PbTe SLs.

spins, the field has to overcome the anisotropy; the field strength needed for that is  $H_{\text{ext}} \sim \sqrt{H_a H_J}$ , where  $H_a$  is the anisotropy field, and  $H_J$  is the exchange field expressed in magnetic units. Since  $H_a$  in EuTe has been found to be about 12 G at 4.2 K, and  $H_J$  is about 3.5 T, the flop to the perpendicular position should occur before  $H_{\text{ext}}$  reaches 650 G. After that, all spins make an  $80^\circ$  angle with the reflecting plane (see Fig. 7(b)), and the reflection intensity is  $I \propto \cos^2 80^\circ = 0.03$ ; in other words, it should drop to 5.9% of its zero-field value. With further  $H_{\text{ext}}$  increase the intensity should not change much until reaching the Tesla region, where the Eu moments start inclining significantly toward the field, leading to further suppression of AFM reflection. However, when the field is gradually decreased, the original zero-field intensity should not be restored, because all the spins should remain 'locked' in the perpendicular position by the anisotropy field.

This idealized model scenario changes quite dramatically for an odd  $m$ . Now, the field tends to align the uncompensated moment parallel to  $\vec{H}_{\text{ext}}$ . The field strength needed to overcome the anisotropy is  $\sim mH_a$ , i.e.,  $\leq 100$  G for the  $m \leq 10$  systems studied by us. In such  $H_{\text{ext}}$ , all the spins get aligned parallel to the  $(11\bar{3})$  plane, so now  $\alpha = 0$  and  $I \propto \cos 0 = 1$ ; in other words, in  $H_{\text{ext}} \approx 100$  G, there should be an increase of the  $(\frac{1}{2}\frac{1}{2}\frac{3}{2})$  reflection intensity by a factor of almost two. After that initial jump, the intensity should not change until the field reaches a value where inclining of the Eu moments from the magnetic field lowers the system energy. After the field returns to zero, the spins should choose easy axes nearest to the field direction, so that the  $S$ -domains corresponding to the  $[11\bar{2}]$  direction should not be repopulated. All spins now make a  $29.5^\circ$  angle with the reflecting plane, so that  $I \propto \cos 29.5^\circ = 0.8$  should be about 60% higher than originally.

As illustrated in Fig. 8, the significant increase of the

reflection intensity, expected to occur in samples with odd  $m$ , was never observed in any real EuTe/PbTe SL. A slight increase ( $\sim 10\%$ ) was observed in some specimens – however, for samples with even  $m$ . Moreover, the observed  $I(H_{\text{ext}})$  characteristics are almost completely reversible – there is no indication for any hysteresis. After the field was increased and then returned back to zero, in all samples the original reflection intensity was restored within experimental error.

All studied samples behaved essentially as in the ‘even- $m$  scenario’ (apart from reversibility), thus showing no uncompensated magnetic moment. However, the field needed to rotate all spins to the direction perpendicular to  $H_{\text{ext}}$  was always significantly higher than the expected value of  $H_{\text{ext}} = \sqrt{H_a H_J} \approx 650$  G, corresponding to the bulk value of  $H_a = 12$  G. Moreover, the shape of the curves in Fig. 8 is not consistent with a single  $H_a$  value, but rather suggest that in each sample there is a statistical distribution of the anisotropy fields. In fact, a satisfactory description of the observed curves was obtained by assuming a Gaussian distribution of the  $H_a$  values. The mean  $H_a$  values obtained from the fits for different samples varied from 50 to 200 G, but no systematic trend has been found. To comment on the fact that no traces of any hysteresis were observed in the studied samples, we recall that the expected ‘even- $m$  scenario’ irreversibility was deduced for idealized, perfect layers with the three-fold symmetry of anisotropy fields as in the bulk material. In real SLs, not only are the values of  $H_a$  different, as obtained from the fits in Fig. 8, but also distribution of their directions may deviate substantially from the  $\langle 211 \rangle$  axes due to the influence of various types of defects and inhomogeneities.

The absence of the ferrimagnetic properties in the SL samples with nominally odd number  $m$  of magnetic monolayers, seen in the  $(\frac{1}{2}\frac{1}{2}\frac{3}{2})$  reflection intensity vs. field strength measurements, was further corroborated by the magnetization studies. In Fig. 9 the magnetic moments for various samples, per SL period, per  $\text{mm}^2$ , are plotted vs. the magnetic field up to 1 kG, which should align all the uncompensated spins parallel to the field. As shown in Fig. 9, for all SL samples, with both nominally even and odd  $m$ , the magnetic moment is several times smaller than the value 340 nanoemu one should observe from the  $1 \text{ mm}^2$  of an uncompensated EuTe monolayer.

The observed field dependence of the intensity of the  $(\frac{1}{2}\frac{1}{2}\frac{3}{2})$  peak, the absence of hysteresis and the low values of the net magnetic moments at intermediate magnetic fields all indicate that the vanishing of the magnetic moments in the SLs with nominally odd numbers of Eu monolayers can neither result from a random orientations of ferrimagnetic domains, nor from an antiparallel orientation of such domains in consecutive EuTe layers due to interlayer coupling. It must result from almost complete compensation of the magnetic moment within each domain. Such an unexpected compensation may be attributed to, e.g., a specific terrace structure of EuTe layers with one monolayer steps as shown in Fig. 10. The

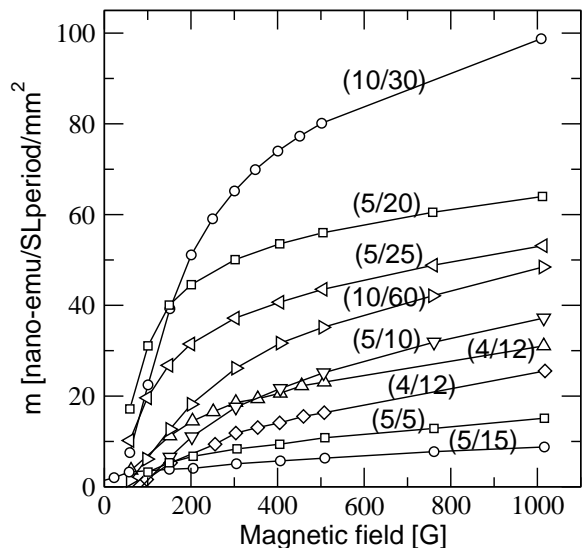


FIG. 9: Magnetic moment per SL period, per  $\text{mm}^2$  for several EuTe/PbTe SLs with nominally odd and even number of magnetic monolayers in EuTe layer vs. applied magnetic field.

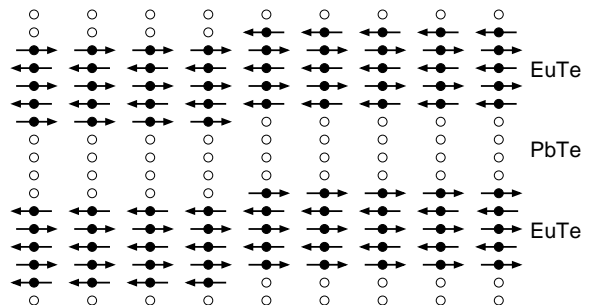


FIG. 10: Diagram of  $(5/4)$  EuTe/PbTe SL with conformally repeated terrace structure, that leads to a large reduction of the total magnetic moment of the individual odd- $m$  EuTe layer as compared with an identical layer without such a step. For clarity, only the cations, Eu (solid circles) and Pb (open circles), are presented and the anion Te atoms are omitted.

existence of one monolayer thick steps on the surface of MBE deposited EuTe layers has been confirmed by scanning tunneling microscopy studies<sup>20</sup>. The X-ray and neutron diffraction spectra, reported in the next section, prove the very high structural quality of our SLs, without traces of any significant interface roughness. They do not exclude, however, such terrace structures, the more so when the steps are conformally repeated over several SL periods.



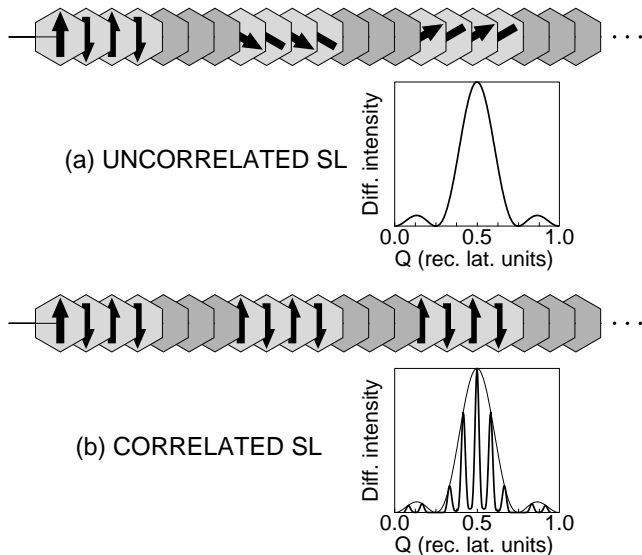


FIG. 11: Possible spin configurations in EuTe/PbTe SLs. (a) Uncorrelated SL; directions of the monolayer magnetizations in consecutive EuTe layers change randomly giving rise to a single broad maximum in a neutron diffraction pattern. (b) Correlated SL; directions of the monolayer magnetizations in consecutive EuTe layers change in a regular way; in the case presented in the Figure, the orientations of the spins in all layers are the same. Corresponding diffraction pattern exhibits a number of narrow fringes.

#### IV. INTERLAYER COUPLING

##### A. Neutron diffraction in zero magnetic field

Magnetic neutron diffraction is the only experimental tool capable of revealing the interlayer spin correlations in the case of AFM/nonmagnetic multilayers. The principle of the method is illustrated in Fig. 11. Neutron diffraction scan along the [111] direction through the  $(\frac{1}{2}\frac{1}{2}\frac{1}{2})$  reflection point from  $[(\text{EuTe})_{10}(\text{PbTe})_{30}]_{300}$  specimen with rather large thickness of the nonmagnetic PbTe spacers ( $d_{\text{PbTe}} = 112\text{\AA}$ ) is displayed in Fig. 12(a). The large number of SL satellite peaks in the X-ray diffraction spectrum and the excellent agreement with dynamical simulations (Fig. 12(b)) prove that the structural quality of the specimen is very high. In contrast to the multi-peaked X-ray pattern, the magnetic neutron diffraction spectrum of this SL has only the form of a single broad peak accompanied by two weak subsidiary side maxima. This profile shows a close similarity to the squared structure factor of a *single*  $(\text{EuTe})_m$  layer,  $|F_{\text{BL}}|^2$ , known from the standard diffraction theory<sup>21</sup> (also see the Appendix). Such a spectrum shape produced by a *multilayer* structure indicates the lack of coherence between the waves scattered by successive layers, meaning that the spin alignments in these layers are not correlated. However, when the PbTe spacer thickness decreases, the character

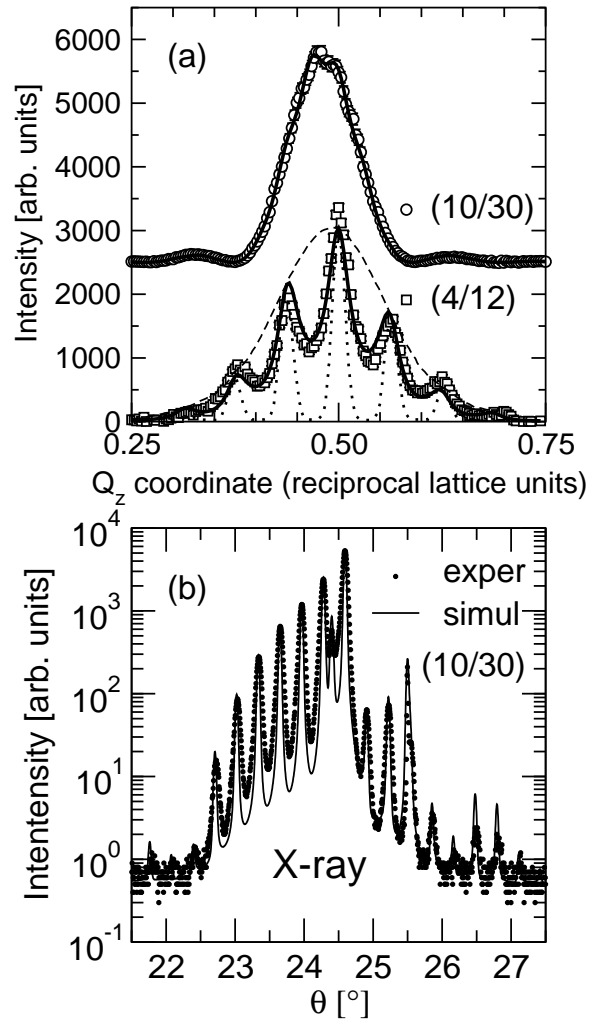


FIG. 12: (a) Neutron diffraction scans along the [111] direction through the principal  $(\frac{1}{2}\frac{1}{2}\frac{1}{2})$  AFM reflection in a 10/30 and 4/12 SL sample, showing pronounced satellite peaks for the latter one. The dotted line represents the expected shape of the spectrum for the fully correlated SL, with the instrumental resolution taken into account. The dashed line shows the single layer magnetic structure factor. (b) High-resolution X-ray diffraction scan through the (222) reflection in the 10/30 SL specimen (points: measured data, line: dynamical simulation).

of the AFM reflections dramatically changes. As exemplified in Fig. 12 for the 4/12 SL, a distinct pattern of narrower satellite peaks then emerges at regular intervals  $\Delta Q_z$  equal to the spacing between the satellite peaks in the X-ray spectra. This clearly indicates the formation of magnetic interlayer correlations across the PbTe spacers. For  $d_{\text{PbTe}}$  below  $\sim 60\text{\AA}$  these magnetic satellites become the dominant part of the spectrum, as is also shown in Fig. 13 for a series of  $[(\text{EuTe})_5(\text{PbTe})_n]_{300}$  SL samples with varying PbTe spacer thickness.

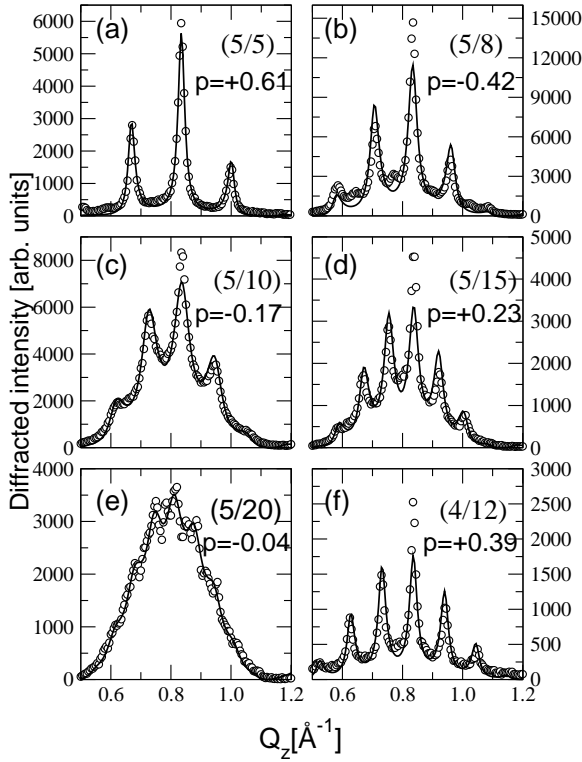


FIG. 13: High resolution magnetic diffraction patterns from several SL samples measured with NG-1 reflectometer. The solid curves are fits of Eq. (9) to the data points. The fitted values of the partial correlation coefficient  $p$  for each spectrum (as defined in subsection D) is shown in the figure. The small additional peaks visible in between the magnetic SL satellites must not be attributed to the correlations of opposite sign - they can as well result from different periodicity in a small portion of the SL (compare Appendix).

### B. Neutron diffraction in high magnetic field

The evolution of the  $(\frac{1}{2}\frac{1}{2}\frac{1}{2})$  reflection for two,  $[(\text{EuTe})_4|(\text{PbTe})_{12}]_{400}$  and  $[(\text{EuTe})_5|(\text{PbTe})_{15}]_{400}$ , SLs in  $\vec{H}_{\text{ext}}$  parallel to the  $[1\bar{1}0]$  axis is presented in Fig. 14. With increasing  $H_{\text{ext}}$ , antiferromagnetically coupled spins first rotate towards directions perpendicular to the field and then gradually incline towards the field (see schemes in Fig. 14). Accordingly, the AFM  $(\frac{1}{2}\frac{1}{2}\frac{1}{2})$  diffraction structure gradually fades away, while a new set of peaks emerges in the (111) FM diffraction region at  $Q_x = 1$ . The almost total disappearance of the AFM component at 6 T is consistent with the behavior of bulk EuTe in external magnetic fields<sup>22</sup>. With respect to the magnetic interlayer coupling, it is crucial to note, that the FM SL peaks at  $Q_z = 1$  are quite narrow (only slightly broadened beyond the instrumental linewidth) as compared to the significantly broader satellite peaks in the AFM region at  $Q_z = 1/2$  and  $B_{\text{ext}} = 0$ . In addition, there is no broad background in the FM region. The sharp satellite peaks in the FM state are due to the perfect long range spin coherence due to spin alignment

by the high external magnetic field, which gives additional clear evidence for the excellent structural quality of the samples. As a consequence, the broadening of the satellite peaks in the AFM region *cannot* be attributed to structural imperfections, but must be due to a limited long range *spin coherency* between the magnetic layers in the AFM state that may be induced only by spontaneous magnetic interlayer interactions.

### C. Field cooled samples

All the above experiments have been carried out on samples which were cooled to temperatures below  $T_N$  in zero external magnetic field. In this case, the magnetic field applied to a sample that is already in a correlated state does not destroy the existing interlayer correlation unless the field becomes strong enough to influence the AFM order within the individual layers. This takes place only for external fields much stronger than 1 T. In contrast, cooling the samples from above to below  $T_N$  in relatively weak magnetic fields (of the order of 100 - 200 G) almost entirely prevents the formation of any interlayer correlations. This is demonstrated in Fig. 15, where the magnetic diffraction patterns obtained for zero-field-cooled (ZFC) and the field-cooled (FC) superlattices are depicted. The magnetic field was applied parallel to the SL growth plane and oriented along the  $[1\bar{1}0]$  crystallographic axis. In the field-cooled cases (open symbols), the spectra only have the form of the structure factor of a single layer  $|F_{\text{BL}}|^2$ , characteristic for uncorrelated SLs (see Fig. 11(a)), whereas the spectra obtained after zero-field cooling show the usual satellite peaks attributed to interlayer coupling (as shown in Fig. 11(b)). This change of the diffraction spectra just by the application of an external field during cooling again demonstrates the purely magnetic origin of the multi-peak structure. Detailed experiments, in which the  $(\frac{1}{2}\frac{1}{2}\frac{1}{2})$  peak profile was studied after cooling the sample in different external fields show that the loss of correlations exhibits a gradual dependence on the field strength. The multi-peak spectrum starts to evolve towards a broad maximum already for cooling at fields as low as 10 G, but the final uncorrelated state is being reached only when cooling at higher fields, usually a few hundred gauss. However, the effect is fully reversible - subsequent warming up and cooling down the samples again in zero field restores the original correlated state. All the samples under investigation have shown this type of behavior.

The possible explanation of the different behavior of the FC and ZFC samples will be given in the next subsection. Here, however, it should be emphasized that such a behavior excludes the possibility that the satellite structure of the  $(\frac{1}{2}\frac{1}{2}\frac{1}{2})$  peak results from the pinholes in the PbTe spacer and the formation of EuTe bridges across the spacer region, because in such case the resulting interlayer coupling would not depend so sensitively on the applied external fields.

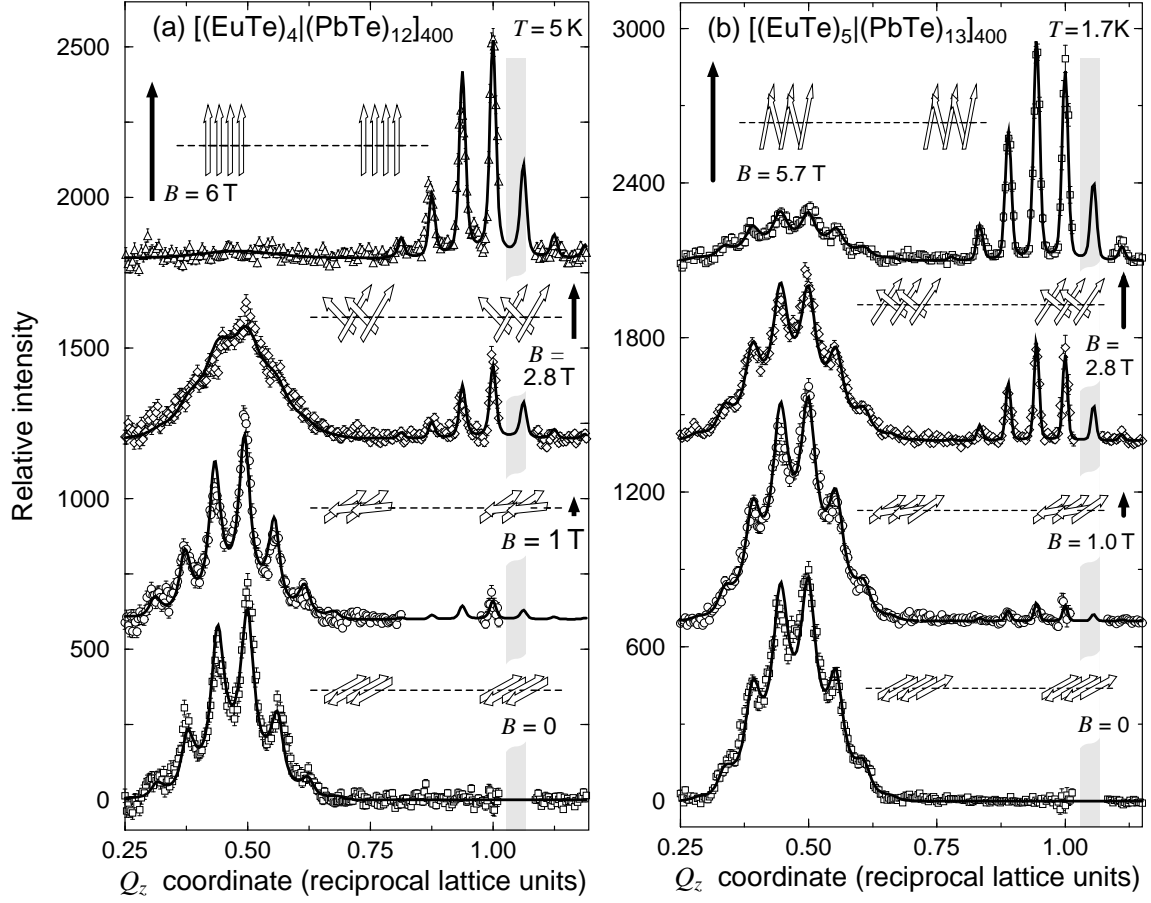


FIG. 14: Extended neutron diffraction scans for (4/12) (a) and (5/13) (b) SL samples, showing the suppression of the AFM scattering at the  $(\frac{1}{2}\frac{1}{2}\frac{1}{2})$  reflection point ( $Q_z = 0.5$ ) with increasing external magnetic fields, and the emerging of new satellite lines near the (111) reciprocal lattice point ( $Q_z = 1.0$ ) due to the induced FM spin alignment (chemical structure contributions are subtracted – the data represent purely magnetic scattering). The shaded bars (removed data points) indicate the regions where a very strong reflection from the  $\text{BaF}_2$  substrate occurs. The solid curves are the best fits of Eq. (9) to the data. The corresponding alignments of magnetization in successive spin monolayers are shown by the arrows.

#### D. Comparison of the experimentally determined interlayer correlations with theoretical predictions.

Three mechanisms of the interlayer correlations, which can be relevant to AFM/nonmagnetic semiconductor layer structures, have been proposed in literature. First, the transfer of the magnetic order to the next magnetic layer via the spin-polarized carriers bound to the impurities located in the spacer, was considered in Refs. 23,24. This does not seem to apply to EuTe/PbTe SLs, since in PbTe the large dielectric constant and small carrier effective masses prevent the formation of shallow impurity centers<sup>25</sup>. Another mechanism considered is the long-range dipolar interaction, which was investigated in Ref. 26 for FM metallic layer systems with domain structure. It does not exist for perfect AFM layers, but one can argue that in real SLs the dipolar coupling between local magnetic moments related to interface terraces and steps as invoked in Section III C, can be effective. We ex-

pect, however, this mechanism to be much weaker here than in the FM case, since the dipole-dipole interaction is proportional to the square of the average dipole moment. In addition, we expect that such mechanism should be much more effective for SLs with odd number of magnetic monolayers than for those with  $m$  even, where the terraces do not lead to local dipole moments. No such preference was observed in the experimental data.

Finally, in Ref. 27 a mechanism was presented, which attributes the interlayer coupling to the sensitivity of the SL electronic energies to the magnetic order in consecutive magnetic layers. The total energy of the valence electrons for two different magnetic SLs, one with the same and the other with opposite spin configurations in neighboring magnetic layers, was compared. The difference between these two energies was considered as a measure of the strength of the interlayer magnetic coupling resulting from band structure effects. In Ref. 27 it was shown that in both studied types of IV-VI semiconductor

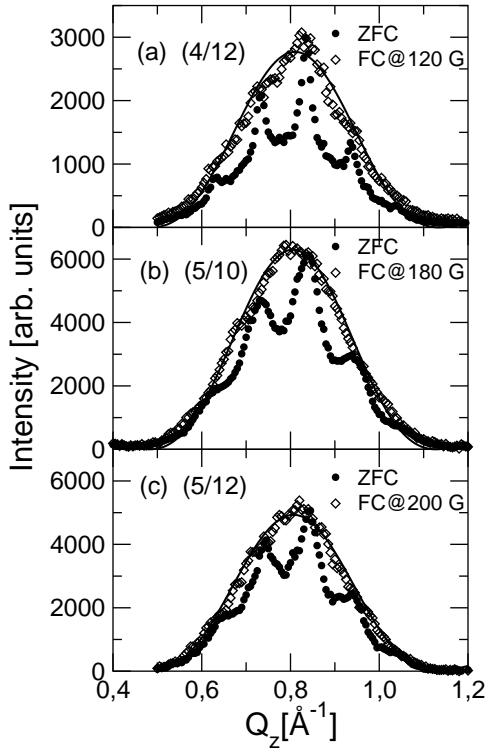


FIG. 15: Neutron diffraction scans performed at  $(\frac{1}{2}, \frac{1}{2}, \frac{1}{2})$  reciprocal lattice position for the zero-field-cooled (ZFC) and field-cooled (FC) (5/10), (5/12), and (4/12) SLs. The FC data has been rescaled to show the effect of enveloping the ZFC data. These diffraction data were collected on the NG-1 reflectometer. The absence of the interlayer correlations in the samples after field cooling is evident (some traces are still visible in the 4/12 sample). For comparison the calculated single layer structure factor is plotted with a continuous line.

structures, i.e., in FM EuS/PbS and AFM EuTe/PbTe, this mechanism can be effective. As shown in Fig. 16, the calculated strength of the coupling decreases monotonically with the increasing thickness  $n$  of the spacer and is practically independent of the thickness  $m$  of magnetic layers. In addition, it was found that for all FM and AFM SLs, regardless of their  $m$  and  $n$  values, the lower energy corresponds to the antiparallel alignment of the two spins facing each other across the spacer layer. In other words, the mechanism leads to an antiferromagnetic coupling between the FM layers. In the AFM EuTe/PbTe structures, however, the energetically preferred spin configuration along the SL growth axis depends on the parity of the number of monolayers within the magnetic layer, i.e., the actual magnetic period is equal to the chemical period for even  $m$  but twice as large for odd  $m$ .

These theoretical results have proven to explain the experimental observations in the FM (001) EuS/PbS SLs<sup>11</sup>. For FM structures the magnetization and neutron reflectivity measurements in external magnetic fields, enable one to determine directly the strength of the coupling and compare it with the model. The sign of the in-

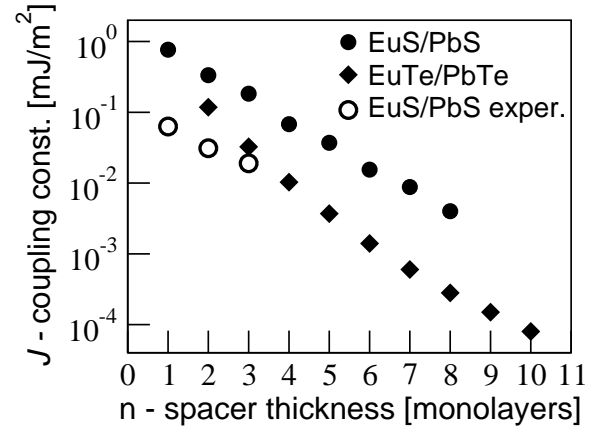


FIG. 16: The interlayer exchange constant  $J$ , defined by the difference of the total electronic energy for the same and opposite spin configurations in successive magnetic layers of the SL, as a function of the spacer thickness for FM EuS/PbS and AFM EuTe/PbTe SLs. Open circles represent the experimentally obtained  $J$  for FM EuS/PbS. For the AFM SLs the direct experimental determination of the strength of the coupling is not possible.

terlayer exchange coupling and the rate of its decrease with the PbS nonmagnetic spacer thickness are in very good agreement with the predictions of the model, as shown in Fig. 16. The fact that the experimental values of the exchange constants estimated from the saturation fields in real FM structures are about an order of magnitude smaller than the theoretical ones was attributed in Ref. 11 to the interfacial roughness and interdiffusion, which were shown to reduce significantly the strength of the interlayer coupling, also in metallic structures.

For the AFM EuTe/PbTe structures the comparison of the theoretical predictions with the experimental data is much more complicated than for the FM structures – in this case not only the perfect tool to measure the strength of the interlayer coupling, i.e., the saturation magnetization, is not applicable, but, as shown below, the correlated spin configurations are much more sensitive to the morphology of the SL.

In our superlattices evidence for the interlayer coupling between the AFM EuTe layers comes from the satellite structure of the neutron diffraction spectra. The sign of the coupling can be determined only by a detailed analysis of the positions of the satellite peaks. Moreover, to describe the observed shapes of the AFM diffraction spectra, we have to invoke the idea of “partial correlations”, described by an interlayer correlation parameter  $p$  ( $|p| < 1$ ), as presented in detail in the Appendix. An idealized fully correlated EuTe/PbTe SL would contain a single  $S$ -domain, with the monolayer magnetization sequence in any  $i^{\text{th}}$  layer either *repeated* in the  $(i + 1)^{\text{th}}$  layer (perfect correlations with  $p = +1$ )

$$\uparrow\downarrow\uparrow\downarrow \dots \uparrow\downarrow\uparrow\downarrow \dots \uparrow\downarrow\uparrow\downarrow \dots \uparrow\downarrow\uparrow\downarrow,$$

or *reversed* in the  $(i + 1)^{\text{th}}$  layer (perfect correlations with

$p = -1$ )

$\uparrow\downarrow\uparrow\downarrow \cdots \downarrow\uparrow\downarrow\uparrow \cdots \uparrow\downarrow\uparrow\downarrow \cdots \downarrow\uparrow\downarrow\uparrow$ .

In both cases, the AFM neutron diffraction pattern should exhibit a series of very narrow peaks, with the width defined by the instrumental resolution only, as seen for the satellite peaks in the FM region at  $H_{\text{ext}} = 6$  T in Fig. 14 and Fig. 11(b). However, in real samples, this perfect long range SL order may be disrupted by “phase lapses” (i.e., switches to the other S-domains types) occurring at random intervals. Such “partially correlated” chains can then be characterized by *fractional*  $p$  values, now expressing the probability  $P = (1 + p)/2$  that any two adjacent EuTe layers have identical spin sequences. Applying diffraction theory to such a system, one obtains the following expression for the magnetic diffraction intensity (see the Appendix for the formula derivation):

$$I(Q_z) \propto |F_{\text{BL}}(Q_z)|^2 \frac{1 - p^2}{1 - 2p \cos(Q_z D) + p^2} \quad (9)$$

where  $D = m\delta_{\text{EuTe}} + n\delta_{\text{PbTe}}$  is the SL period;  $\delta_{\text{EuTe}}$  and  $\delta_{\text{PbTe}}$  being the monolayer thicknesses of EuTe and PbTe, respectively. This expression is similar to that used for analyzing x-ray diffraction patterns from partially ordered layered structures<sup>28</sup>. The value of  $p$  determines both the widths of the AFM satellite peaks as well as the height of the underlying “hump” (see Fig. 17). By adjusting the  $p$  parameter for each sample the observed spectral shapes are reproduced remarkably well (solid lines in Fig. 13). The least-square fitted  $|p|$  values are considerably lower than unity, even for relatively thin PbTe spacers. This indicates the presence of mechanisms inhibiting the correlation formation in the AFM EuTe/PbTe SLs. Although one can speculate that several effects, such as thickness fluctuations or interface roughness, may participate in the suppression, neutron diffraction measurements in moderate external in-plane fields  $H_{\text{ext}} < 1$  T imply that magnetic anisotropy fields  $H_a$  in random directions parallel to the layers play a major role in this effect. Two  $S$ -domains in EuTe layers facing each other across the nonmagnetic spacer may become correlated only if the interlayer coupling energy is sufficiently high to overcome the anisotropy in at least one of them.

This observation together with the model described above offers a simple qualitative explanation of the behavior of the field cooled samples shown in Fig. 15. It is based on the fact that the interlayer coupling becomes effective only below the Néel temperature, when the AFM order in EuTe layers is already well established and the anisotropy fields are still weak. The interlayer coupling energy resulting from band structure effects is proportional to the cosine of the angle  $\theta$  between the spins at the opposite borders of the nonmagnetic spacer. Thus, the torque responsible for the relative rotations of the spins in neighboring EuTe layers should be proportional to  $\sin \theta$ . During cooling of the sample in an external mag-

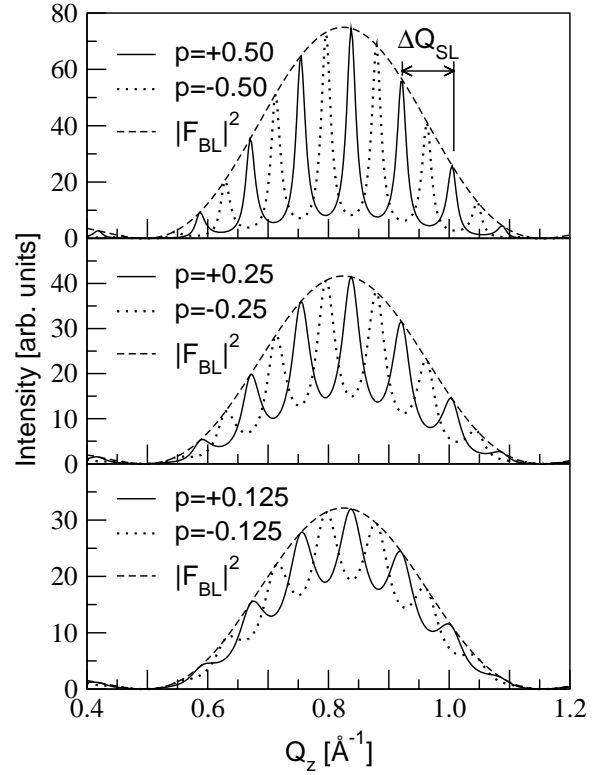


FIG. 17: Influence of the magnitude and the sign of the correlation parameter  $p$  on the magnetic diffraction intensity from 5/15 SL, as calculated from Eq. (9). The change of the sign of  $p$  leads to the shift of the SL satellite peaks by half of the spectrum periodicity. With the decreasing value of  $|p|$  the width of the peaks increases and so does the height of the underlying “hump”. The single EuTe layer magnetic structure factor  $|F_{\text{BL}}|^2$ , enveloping the whole spectrum, is presented with the dashed line.

netic field, all the spins align along the direction perpendicular to the magnetic field. Thus, the torque is equal to zero and the interlayer correlations cannot be formed. In contrast, in the ZFC samples the AFM ordered spins in different magnetic layers align randomly along different in-plane directions, hence  $\sin \theta$  and the torques are in general not equal to zero. Therefore, the rotation mechanism can be effective, leading to the correlated layer structure in the case of ZFC samples.

From Eq. (9) and Fig. 17 it follows that for a given combination of  $m$  and  $n$  values the change of the  $p$  sign corresponds to a half period shift  $\frac{1}{2}\Delta Q_{\text{SL}}$  in the AFM satellite positions. For  $Q_z$ 's in the vicinity of  $(\frac{1}{2}\frac{1}{2}\frac{1}{2})$  reciprocal lattice point the same is expected when the  $p$  is fixed, but either  $m$  or  $n$  is changed by  $\pm 1$ . This allows one to determine the relative spin configurations in successive layers in the SLs from the obtained sign of the interlayer coefficient. We note that this is possible under a strong assumption that the structures are morphologically perfect, i.e., with the same, well defined  $m$  and  $n$  values throughout the entire  $(\text{EuTe})_m|(\text{PbTe})_n$  SL composed of several hundreds of periods. From such an anal-

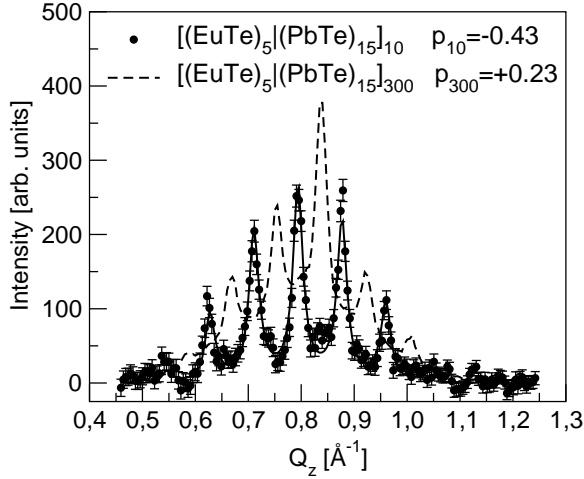


FIG. 18: Magnetic diffraction pattern from highly perfect EuTe/PbTe  $(5/15) \times 10$  SL (circulated solid line) showing the strong interlayer correlation. In this case the negative sign of  $p$  is in agreement with the theoretical model predictions. The experimental data for the less perfect SL with 300 repetitions (dashed line) is shown for comparison.

ysis it turned out that the spectra for the superlattices with nominally even  $m$  and even  $n$  reveal the preference for the same monolayer spin sequence in successive EuTe layers ( $\cdots \uparrow\downarrow \cdots \uparrow\downarrow \cdots$ ). For SLs with odd  $m$  and even  $n$  neutron diffraction spectra indicated reversed configuration ( $\cdots \uparrow\downarrow\uparrow \cdots \downarrow\uparrow\downarrow \cdots$ ). Both these configurations are in agreement with the theoretical model prediction. In contrast, for the samples with  $m$  and  $n$  both nominally odd, the neutron diffraction spectra seem to indicate that the ( $\cdots \uparrow\downarrow\uparrow \cdots \uparrow\downarrow\uparrow \cdots$ ) configuration is preferred, contrary to the theoretical results.

To shed light on this issue, an effort to detect the interlayer exchange coupling in EuTe/PbTe SLs with a smaller number of SL periods, i.e., in SLs with better controlled  $m$  and  $n$  values, was undertaken. This task is not trivial as the intensity of neutron diffraction spectrum depends crucially on the number of spins involved. From the additional series of EuTe/PbTe SLs with only 10 periods, one sample indeed showed SL satellite peaks in positions corresponding to the sign of the coupling predicted by the model. In Fig. 18 we present the comparison of the spectra of two SLs, both with nominal  $m = 5$  and  $n = 15$ , and with different number of SL periods  $N$ . Clearly, the sample with only 10 periods shows the expected negative  $p$  value as compared to the opposite sign for the previously measured sample with 300 periods (dashed line in Fig. 18). This result seems to suggest that in the long process of MBE growth of the SLs with a large number of repetitions (typical growth time of several hours) the preference occurs to form terraces with even number of monolayers. The reasons leading to such tendency remain unclear, but one conceivable explanation may be that the number of monolayers which form a unit cell of the bulk material is somehow preferred during the long

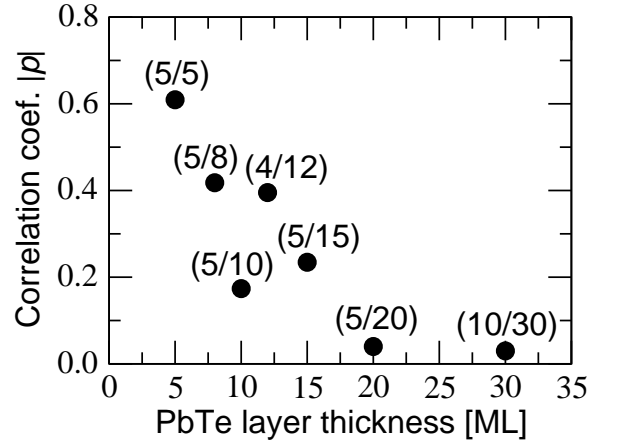


FIG. 19: Dependence of the interlayer correlation parameter  $p$  on the PbTe spacer thickness in EuTe/PbTe superlattices as determined from the fitting of the neutron diffraction spectra.

process of layer growth. In the  $[111]$  direction this corresponds to two cation and two anion sheets. Such a mechanism would be valid for both, EuTe and PbTe, constituent materials.

The theoretically predicted decrease of the strength of the coupling with the nonmagnetic spacer thickness is reflected in the decrease of the values of the correlation coefficient  $p$ , as shown in Fig. 19. A quantitative comparison between the experimental and theoretical results is not possible in this respect. As far as the range of the interaction is concerned, the experimentally observed very long range of the interlayer interactions seems to exceed the range predicted by the model. The weak correlations still visible in samples with very thick spacers can be ascribed to the possible contribution from a residual dipole-dipole interaction.

## V. CONCLUSIONS

We have performed an extensive study of the magnetic properties of AFM EuTe epitaxial layers and of  $[(\text{EuTe})_m | (\text{PbTe})_n]_N$  SLs grown by molecular beam epitaxy along the  $[111]$  direction. The structural properties of these samples were characterized by high resolution x-ray diffraction. The magnetization and neutron diffraction experiments show that the magnetic properties of the type II AFM EuTe layers depend sensitively on lattice distortions stemming from EuTe/PbTe lattice constant mismatch. Due to the resulting biaxial strain and finite EuTe layer thickness, the FM spin-sheets are all oriented parallel to the  $(111)$  growth plane, i.e., they form a single  $T$ -domain.

For a large number of EuTe/PbTe SLs, a systematic study of the Néel temperature dependence on the number of EuTe and PbTe monolayers in the SL period was performed. The transition temperature to the AFM phase depends on the strain state of the magnetic layers as well

as on their finite thickness. The observed changes of the Néel temperature are described by the dependence of the exchange parameters on the lattice distortions and they follow essentially a mean field behavior.

From neutron diffraction measurements in an applied magnetic field parallel to the (111) growth plane, detailed information on the  $S$ -type domain structure and on the in-plane anisotropy fields was obtained. The latter ones are considerably higher than in bulk EuTe. These fields play an important role in the formation of interlayer correlations. Neutron diffraction experiments in moderate magnetic fields and magnetization measurements showed that, irrespective of the number of monolayers in the EuTe layer, no net magnetic moment is present in the studied SLs. In this sense the EuTe/PbTe system constitutes a prototypical example of an antiferromagnetic/diamagnetic superlattice.

The most interesting feature of these SLs is a pronounced interlayer spin correlation between successive EuTe layers revealed by magnetic neutron diffraction. The characteristic fingerprint of these correlations are SL satellite peaks in the vicinity of  $(\frac{1}{2}\frac{1}{2}\frac{1}{2})$  reciprocal lattice point. The correlations persist up to PbTe layer thicknesses of about 60 Å. Based on kinematical diffraction theory, the formula describing the diffracted beam intensity as a function of momentum transfer,  $Q_z$ , has been derived for a general case of partially correlated SLs. A correlation parameter  $p$  (obtained by least-square-fitting to the neutron diffraction spectra) was found to follow a downward trend with increasing thickness of the non-magnetic spacer layer, thus, reflecting the weakening of the interlayer interactions with the distance between the magnetic layers. The signs of  $p$  – that govern the spin sequences in successive EuTe layers – were compared with the predictions of the theoretical model presented in Ref. 27. In this model the interlayer correlations are mediated by valence-band electrons and are inferred from the minimization of the total electronic energy of the EuTe/PbTe system on the spin arrangements in adjacent magnetic layers. Essentially, the major features of this theoretical model, namely:

- (i) monotonic decay of the interlayer interactions with the distance between magnetic layers,
- (ii) independence of coupling strength on magnetic layer thickness, and
- (iii) opposite directions of the spins in the bounding monolayers of the two consecutive EuTe layers facing each other across the PbTe spacer

have been confirmed in our neutron and magnetization experiments, although in order to be able to check experimentally the last issue (especially for  $m$  – odd/ $n$  – odd SLs) samples with extreme structural perfection were necessary.

## APPENDIX: NEUTRON DIFFRACTION SPECTRUM FOR AFM SUPERLATTICES

In this Appendix we calculate the profiles of diffraction spectra for a SL made up of alternating  $N$  antiferromagnetic layers and  $N$  nonmagnetic layers, each consisting of  $m$  and  $n$  atomic monolayers, respectively. For simplicity, in the following it is assumed that in both SL constituent materials the spacing between the monolayers has the same value of  $d$  and that there are only two possible directions of spin (magnetization) in each magnetic monolayer (it can be shown, however, that the results of this Appendix remain valid for systems with several in-plane easy axes and for layers consisting of many  $S$ -domains<sup>29</sup>).

We consider three different situations:

- (a) *perfectly correlated SLs* – interlayer correlations lead to one of the two types of magnetic order, illustrated in the diagrams in Section IV D, in the entire SL;
- (b) *uncorrelated SLs*; and
- (c) *partially correlated SLs* – structures, in which there is a dominant tendency to form one type of correlations between the successive magnetic layers, but due to some disruptive mechanisms a minority of nearest-neighbor layers pairs is aligned in the opposite way.

In the standard kinematical theory approach the diffracted wave, resulting from magnetic scattering of unpolarized neutrons, is obtained by adding up all waves diffracted by individual magnetic atoms. This leads to the following equation:

$$\psi_{\text{diff}} \propto f(Q) \sum_j \kappa_j \exp(i\vec{Q} \cdot \vec{r}_j) \quad (\text{A.1})$$

where  $\vec{Q}$  is the scattering vector,  $f(Q)$  is the single-atom magnetic formfactor,  $\vec{r}_j$  is the position of the  $j^{\text{th}}$  atom, and  $\kappa_j$  is the magnetic scattering amplitude for a single atom, equal  $+\kappa$  or  $-\kappa$  for the “up” and “down” spin orientation, respectively. In the symmetric reflection geometry, most often used in diffraction studies of multilayers, the scattering vector is parallel to the superlattice axis:  $\vec{Q} = (0, 0, Q_z)$ . The summation over individual atoms can be then replaced by a summation over the monolayers. Since for all atoms located in the  $l^{\text{th}}$  monolayer  $\vec{Q} \cdot \vec{r}_j = Q_z \cdot z = Q_z l d$ , the equation simplifies to:

$$\psi_{\text{diff}} \propto f(Q) \sum_l \mathcal{M}_l \exp(iQ_z l d) \quad (\text{A.2})$$

where  $\mathcal{M}_l$ , the sum of magnetic scattering amplitudes of all atoms residing in the  $l^{\text{th}}$  monolayer, is proportional to the monolayer magnetization. Taking advantage of the SL periodicity, one can separate this equation into a summation over all monolayers within a SL “elementary

cell” – a bilayer (BL) – and over the  $N$  SL repeats. Thus, for a bilayer, consisting of  $m$  magnetic monolayers (and  $n$  nonmagnetic ones, for which all the  $\mathcal{M}_l = 0$ ), one can define the magnetic structure factor  $F_{\text{BL}}$  as:

$$F_{\text{BL}}(Q_z) \equiv f(Q) \sum_{\mu=0}^{m-1} \mathcal{M}_\mu \exp(iQ_z \mu d) \quad (\text{A.3})$$

Eq. (A.2) can thus be written in the form:

$$\psi_{\text{diff}} \propto F_{\text{BL}}(Q_z) \times \sum_{\nu=0}^{N-1} \xi_\nu \exp(iQ_z D \nu) \quad (\text{A.4})$$

where  $D = (m+n)d$  is the SL period. The spin configuration in the  $\nu^{\text{th}}$  magnetic layer with respect to the first layer is described in Eq. (A.4) by the  $\xi_\nu$  coefficient, which takes the value  $+1$  for the same and  $-1$  for the opposite magnetization sequences.

The intensity  $I(Q_z)$  of the diffracted radiation is given by:

$$|\psi_{\text{diff}}|^2 \propto \sum_{\alpha=0}^{N-1} \sum_{\beta=0}^{N-1} \xi_\alpha \xi_\beta \exp[iQ_z(\alpha - \beta)] |F_{\text{BL}}(Q_z)|^2 \quad (\text{A.5})$$

where the structure factor square  $|F_{\text{BL}}(Q_z)|^2$  can be written as:

$$|F_{\text{BL}}(Q_z)|^2 \propto \begin{cases} \frac{\cos^2(mQ_z d/2)}{\cos^2(Q_z d/2)} & \text{for } m \text{ odd} \\ \frac{\sin^2(mQ_z d/2)}{\cos^2(Q_z d/2)} & \text{for } m \text{ even} \end{cases} \quad (\text{A.6})$$

The structure factor term  $|F_{\text{BL}}(Q_z)|^2$  has broad maxima (with weak subsidiaries on both sides) centered at

$Q_z = \frac{1}{2}(2\pi/d), \frac{3}{2}(2\pi/d), \dots$ , i.e., half-way in between the reciprocal lattice points corresponding to the basic atomic structure with periodicity  $d$ .

Calculating the spectrum profiles  $I(Q_z)$  for SLs with *perfect interlayer correlations* requires putting in Eq. (A.5)  $\xi_\nu$  appropriate for the given type of correlation. The task reduces then to summing geometric progressions, which yields: for  $\xi_\nu = 1$

$$I(Q_z) \propto |F_{\text{BL}}(Q_z)|^2 \frac{\sin^2(NQ_z D/2)}{\sin^2(Q_z D/2)} \quad (\text{A.7a})$$

and for  $\xi_\nu = (-1)^{\nu+1}$

$$I(Q_z) \propto |F_{\text{BL}}(Q_z)|^2 \times \begin{cases} \frac{\cos^2(NQ_z D/2)}{\cos^2(Q_z D/2)} & \text{for } N \text{ odd} \\ \frac{\sin^2(NQ_z D/2)}{\cos^2(Q_z D/2)} & \text{for } N \text{ even} \end{cases} \quad (\text{A.7b})$$

These functions consist of sharp maxima at regular intervals  $\Delta Q_z = 2\pi/D$ . The intensity of the narrow lines is “modulated” by the structure factor, what produces the characteristic groups of peaks. It should be noted that a change from one to another type of interlayer correlations causes the narrow line positions to shift by  $\frac{1}{2}\Delta Q_z$ , which makes possible to detect such a transition.

In order to analyze *uncorrelated* and *partially correlated* SLs the double sum in Eq. (A.5) should be rearranged into sums over different kinds of layer pairs: namely, the sum of all same-layer terms ( $\alpha = \beta$ ), the sum of all terms with  $|\alpha - \beta| = 1$  (i.e., corresponding to adjacent magnetic layers), all terms with  $|\alpha - \beta| = 2$  (i.e., corresponding to next-nearest layer pairs), and so on:

$$\begin{aligned} & \sum_{\alpha=0}^{N-1} \sum_{\beta=0}^{N-1} \xi_\alpha \xi_\beta \exp[iQ_z(\alpha - \beta)] = N + \sum_{\alpha \neq \beta} \xi_\alpha \xi_\beta \cos[Q_z D(\alpha - \beta)] \\ & = N + 2 \cos(Q_z D) \sum_{\alpha=0}^{N-2} \xi_\alpha \xi_{\alpha+1} + 2 \cos(2Q_z D) \sum_{\alpha=0}^{N-3} \xi_\alpha \xi_{\alpha+2} + \dots + 2 \cos[(N-1)Q_z D] \xi_0 \xi_{N-1} \end{aligned} \quad (\text{A.8})$$

The  $\xi_\alpha \xi_\beta$  product for any pair of layers, labeled  $\alpha$  and  $\beta$ , can be thought of as the *correlation coefficient* for this pair. The number of layer pairs that are  $kD$  apart is  $N - k$ ; hence, the average correlation coefficient for all such pairs in the SL structure can be written as:

$$p_k \equiv \langle \xi_\alpha \xi_{\alpha+k} \rangle = \frac{1}{N-k} \sum_{\alpha=0}^{N-k-1} \xi_\alpha \xi_{\alpha+k} \quad (\text{A.9})$$

Using Eqs. (A.8) and (A.9) one can write the Eq. (A.5)

for diffracted intensity in a simple form:

$$I(Q_z) \propto N |F_{\text{BL}}|^2 \left[ 1 + 2 \sum_{k=1}^{N-2} p_k \left(1 - \frac{k}{N}\right) \cos(Q_z D k) \right] \quad (\text{A.10})$$

For a “perfectly random” superlattice the correlation coefficients for all layer pairs vanish on statistical averaging. Hence, for the *uncorrelated* system:

$$I(Q_z) \propto N |F_{\text{BL}}(Q_z)|^2 \quad (\text{A.11})$$



i.e., the diffraction spectrum reproduces the shape of the structure factor square – in agreement with the expected result for a random system with no coherence between the waves scattered by individual layers.

The last situation to discuss is the *partially correlated* superlattice. If it is assumed that the only relevant interactions are between the nearest layers, and there are no long-range interactions, which introduce coupling between the more distant layer pairs, then it is straightforward to show that the correlation coefficient for second-nearest layers is  $p_2 = p_1^2$ , for third-nearest layers is  $p_3 = p_1^3$ , etc. In the following we drop the subscript and denote  $p_1$  by  $p$ .

If the value of  $|p|$  is significantly lower than 1, the correlation coefficients rapidly decrease, and only the first few terms in the sum in Eq. (A.10) are relevant. If, in addition, the number of repeats  $N$  in the SL is large, one can use the approximation  $1 - k/N \cong 1$ , and obtain:

$$I(Q_z) \propto |F_{\text{BL}}(Q_z)|^2 \left[ 1 + 2 \sum_{k=1}^{\infty} p^k \cos(Q_z D k) \right] \quad (\text{A.12})$$

By applying the identity<sup>30</sup>:

$$1 + 2 \sum_{k=1}^{\infty} p^k \cos(kx) = \frac{1 - p^2}{1 - 2p \cos(x) + p^2}$$

one obtains the final formula for the spectrum profile:

$$I(Q_z) \propto |F_{\text{BL}}(Q_z)|^2 \frac{1 - p^2}{1 - 2p \cos(Q_z D) + p^2} \quad (\text{A.13})$$

## ACKNOWLEDGMENTS

Work supported by projects: NSF DMR-0204105, FWF, Vienna, Austria, GME, Vienna, Austria, Austrian Academy of Sciences (APACS), FENIKS project (EC:G5RD-CT-2001-00535) and the Polish State Committee for Scientific Research grant PBZ-KBN-044/P03/2001. The collaboration with J. K. Furdyna and M. S. Dresselhaus and their contribution to the initial stage of these studies is acknowledged.

\* Electronic address: Henryk.Kepa@fuw.edu.pl

† deceased

‡ Present address: Institut für Experimentalphysik, Karl Franzens Universität, A-8010 Graz, Austria

<sup>1</sup> P. Grünberg, R. Schreiber, Y. Pang, M. B. Brodsky and H. Sowers, *Phys. Rev. Lett.* **57**, 2442 (1986).

<sup>2</sup> S. S. P. Parkin, *Phys. Rev. Lett.* **67**, 3598 (1991).

<sup>3</sup> S. Toscano, H. Hopster, and M. Landolt, *J. Mag. Magn. Mater.* **114**, L6 (1992).

<sup>4</sup> L. Briner and M. Landolt, *Phys. Rev. Lett.* **73**, 340 (1994), and references therein.

<sup>5</sup> P. Bruno, *Phys. Rev. B* **52**, 411 (1995), and references therein.

<sup>6</sup> T. M. Giebultowicz, V. Nunez, G. Springholz, G. Bauer, J. Chen, M. S. Dresselhaus, and J. K. Furdyna, *J. Mag. Magn. Mater.* **140-144**, 635 (1995).

<sup>7</sup> V. Nunez, T. M. Giebultowicz, W. Faschinger, G. Bauer, H. Sitter, J. K. Furdyna, *J. Mag. Magn. Mater.* **140-144**, 633 (1995).

<sup>8</sup> J. J. Rhyne, J. Lin, J. K. Furdyna and T. M. Giebultowicz, *J. Mag. Magn. Mater.* **177-181**, 1195 (1998).

<sup>9</sup> H. Kępa, K. I. Goldman, T. M. Giebultowicz, C. F. Majkrzak, G. Springholz, H. Krenn, S. Holl, F. Schinagl, G. Bauer, *Physica E*, **2**, 399 (1998).

<sup>10</sup> K. I. Goldman, G. Springholz, H. Kępa, T. M. Giebultowicz, C. F. Majkrzak, G. Bauer, *Physica B*, **241-243**, 710 (1998).

<sup>11</sup> H. Kępa, J. Kutner-Pielaszek, J. Blinowski, A. Twardowski, C. F. Majkrzak, T. Story, P. Kacman, R. R. Gałazka, K. Ha, H. J. M. Swagten, W. J. M. de Jonge, A. Yu. Sipatov, V. Volobuyev, T. M. Giebultowicz, *Euro-*

*phys. Lett.* **56**, 54 (2001).

<sup>12</sup> P. Wachter, *Handbook on the Physics and Chemistry of Rare Earths* (K. A. Gschneidner and L. Eyring, North Holland, 1979), p. 507.

<sup>13</sup> T. Hihara and M. Kawakami, *J. Phys. Soc. Japan*, **57**, 1094 (1988)

<sup>14</sup> G. Will, S. J. Pickart, H. A. Alperin, and R. Nathans, *J. Phys. Chem. Solids*, **24**, 1679 (1963).

<sup>15</sup> G. Springholz and G. Bauer, *Appl. Phys. Lett.* **62**, 2399 (1993); J. J. Chen et al., *Phys. Rev. B* **54**, 402 (1996).

<sup>16</sup> S. Holl, *J. Mag. Magn. Mater.* **220**, 293 (2000); PhD Thesis, Johannes Kepler Universität, Linz, 2000.

<sup>17</sup> I. N. Goncharenko and I. Mirebeau, *Phys. Rev. Lett.* **80**, 1082 (1998).

<sup>18</sup> D. Kostyk, Y. Shapira, E. J. McNiff, Jr., T. Q. Vu, and A. Twardowski, *Sol. State Commun.* **92**, 473 (1994).

<sup>19</sup> A. Stachow-Wojcik, T. Story, W. Dobrowolski, M. Arciszewska, R. R. Gałazka, M. W. Kreijveld, C. H. W. Swüste, H. M. J. Swagten, W. J. M. de Jonge, A. Twardowski, and A. Yu. Sipatov, *Phys. Rev. B* **60**, 15220 (1999).

<sup>20</sup> G. Springholz, G. Bauer, and V. Holy, *Phys. Rev. B* **54**, 4500 (1996).

<sup>21</sup> R. W. Erwin, J. J. Rhyne, M. B. Salamon, J. Borchers, Shantanu Sinha, R. Du, J. E. Cunningham, C. P. Flynn, *Phys. Rev. B*, **35**, 6808 (1987).

<sup>22</sup> N. F. Oliveira Jr., S. Foner, Y. Shapira, and T. B. Reed, *Phys. Rev. B* **5**, 2634 (1972).

<sup>23</sup> P. Shevchenko, L. Swierkowski, J. Oitmaa, *J. Mag. Magn. Mater.* **177-181**, 1168 (1998).

<sup>24</sup> T. M. Rusin, *Phys. Rev. B* **58**, 2107, (1998-II).

<sup>25</sup> H. Heinrich in *Lectures Notes in Physics*, Vol. **133**

- (Springer-Verlag, Heidelberg, 1980) p.407.
- <sup>26</sup> J. Borchers, P. M. Gehring, R. W. Erwin, J. F. Ankner, C. F. Majkrzak, T. L. Hylton, K. R. Coffey, M. A. Parker, and J. K. Howard, Phys. Rev. B **54**, 9870 (1996).
- <sup>27</sup> J. Blinowski and P. Kacmar, Phys. Rev. B **64** 045302 (2001).
- <sup>28</sup> S. Hendrics and E. Teller, J. Chem. Phys. **10**, 147 (1942)
- <sup>29</sup> K. I. Goldman, H. Kępa, T. M. Giebultowicz, unpublished.
- <sup>30</sup> W. Magnus, F. Oberhettinger, *Formeln und Sätze für die speziellen Funktionen der mathematischen Physik*, Springer-Verlag, Berlin-Göttingen-Heidelberg, 1948.